Available online at www.sciencedirect.com
ScienceDirect
Journal of Sound and Vibration 311 (2008) 254–268
JOURNAL OF SOUND AND VIBRATION
www.elsevier.com/locate/jsvi

Rapid calculation of the compression wave generated by a train entering a tunnel with a vented hood: Short hoods

M.S. Howe[a,*], A. Winslow[a], M. Iida[b], T. Fukuda[b]

[a]*Boston University, College of Engineering, 110 Cummington Street, Boston, MA 02215, USA*
[b]*Railway Technical Research Institute, 2-8-38 Hikari-cho, Kokubunji-shi, Tokyo 185-8540, Japan*

Received 29 March 2006; received in revised form 22 August 2007; accepted 10 September 2007
Available online 26 October 2007

Abstract

A numerical procedure for the rapid prediction of the compression wave generated by a high-speed train entering a tunnel was presented and validated by Howe et al. [Rapid calculation of the compression wave generated by a train entering a tunnel with a vented hood, *Journal of Sound and Vibration* 297 (2006) 267–292]. The method was devised to deal principally with compression wave generation in long hoods typically of length ~10 times the tunnel height and 'vented' by means of a series of windows distributed along the hood walls. Hoods of this kind will be needed to control wave generation by newer trains operating at speeds U exceeding about 350 km/h. In this paper experimental results are presented and compared with predictions in order to extend the range of applicability of the numerical method of Howe et al. (2006) to include short hoods with lengths as small as just twice the tunnel height (the situation for most hoods currently deployed on the Japanese *Shinkansen*) and for U as large as 400 km/h.

1. Introduction

The overall pressure rise across the front of the compression wave generated when a high-speed train enters a tunnel varies roughly as the square of the train speed U and can exceed two or three per cent of atmospheric pressure. The strength of the acoustic pulse (or 'micro-pressure wave') radiated from the far end of the tunnel when the compression wave arrives is proportional to the slope of the compression wave-front and varies as U^3 for short tunnels. It can be large enough to cause 'rattles' in buildings close to the tunnel exit, and its annoyance is increased by the occurrence of nonlinear steepening of the front in modern long 'smooth' tunnels, which causes the pulse to emerge as a sudden, explosive 'bang'. A well-established compression-wave countermeasure involves the installation of an entrance 'hood', which usually consists of a thin-walled extension of the tunnel portal with windows distributed along its length. High-pressure air forced out of the windows by the entering train can cause the initial rise time of the wave to be significantly increased and produce a more 'gently' rising wave-front profile. Further details of the history of hood development together with an extensive bibliography are given by Howe et al. [1].

*Corresponding author. Tel.: +1 617 484 0656; fax: +1 617 353 5866.
E-mail addresses: mshowe@bu.edu (M.S. Howe), iida@rtri.or.jp (M. Iida).

0022-460X/$ - see front matter © 2007 Elsevier Ltd. All rights reserved.
doi:10.1016/j.jsv.2007.09.012

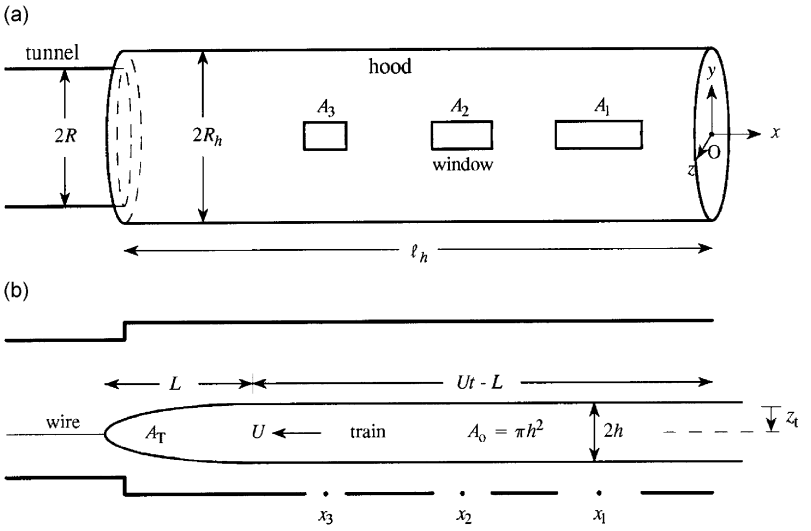

Fig. 1. Parameters defining the configuration of the hood, tunnel and axisymmetric train: (a) 'side' view from the direction of the positive z-axis; (b) 'top' view from the direction of the positive y-axis.

A very efficient numerical algorithm (hereinafter referred to as the 'rapid' algorithm) was introduced in Ref. [1] for calculating the initial form of the compression wave prior to the onset of nonlinear steepening. The algorithm executes in a few seconds on a conventional desktop computer and takes explicit account on wave formation of: (i) the hood-tunnel junction and the accompanying temporary 'trapping' of wave energy by multiple reflections between the ends of the hood, (ii) the forcing of air out of the windows, and (iii) the frictional drag on the train and tunnel walls. The method was validated by comparison with experiments performed at model scale using a circular cylindrical tunnel of interior radius R fitted axisymmetrically with a thin-walled, circular cylindrical, unflanged hood of interior radius R_h and length ℓ_h (see Fig. 1). It was originally devised specifically for application to acoustically *noncompact* hoods, wherein the thickness of the compression wave-front $\leqslant \ell_h$. This was examined experimentally in Ref. [1] by considering only long hoods with $\ell_h = 10R$ that are effective at train speeds $U > 350$ km/h that will be typical in the near future. Predictions were found to be in good agreement with data derived from a series of experiments conducted over a period of years with U as large as 425 km/h.

However, regular train speeds in Japan are already approaching 350 km/h, whereas much of the high-speed network is equipped with 'short' hoods with $\ell_h \sim 2R$ that have been optimized for lower speed operations. It is therefore of great practical interest to examine the extent to which the rapid prediction method of Ref. [1] can be applied to short hoods. In this paper, we report a successful comparison of predictions with a new set of measurements of compression wave formation in short vented and unvented hoods at $U = 350$ and 400 km/h. It is concluded for these speeds that it is *never* legitimate to treat the hood as a compact acoustic element when ℓ_h is as small as $2R$.

The configurations of the experimental hood, tunnel and train are defined in Section 2, and the experimental procedure is outlined in Section 3. Comparisons of theory and experiment for unvented hoods are presented in Section 4, including a discussion of the compact-hood approximation. Short vented hoods are discussed in Section 5.

2. The model scale configuration

2.1. Specification of the short hoods

Take the origin of coordinates (x, y, z) at the centre O of the hood entrance plane as in Fig. 1, with the negative x-axis along the common axis of symmetry of the tunnel and hood. Each window is nominally

rectangular with sides of length ℓ_x parallel to the tunnel axis and ℓ_θ in the azimuthal direction. For the case illustrated in the figure there are three windows distributed in a single row along the hood wall, with the centroid of the kth window of area A_k $(=\ell_{xk}\times\ell_{\theta k})$ at $(x_k, 0, R_h)$, $-\ell_h<x_k<0$ (along the line of intersection of the xz-plane in $z>0$ with the hood). In the usual arrangement an axisymmetric model train is projected into the tunnel along a tightly stretched wire that passes smoothly through a cylindrical channel along the train axis. The 'top' view in Fig. 1b shows the wire displaced a distance $z_t>0$ from the tunnel axis *towards the windows* in the z-direction. The two cases $z_t>0$ ($z_t<0$) therefore correspond, respectively, to a train travelling along near (far) tracks relative to the windows.

To calculate the compression wave prior to the onset of nonlinearity the tunnel is assumed to extend to $x=-\infty$. To a good approximation predictions are independent of window *shape* when $\ell_x\sim\ell_\theta$ and $\ell_x\ell_\theta\ll\mathscr{A}_h\equiv\pi R_h^2=$ hood cross-sectional area. Long, slit-like windows must be approximated by a linear sequence of small windows. The compression-wave algorithm of [1] will be applied to the three short hoods illustrated in Fig. 2, involving a model scale tunnel in the form of a circular cylindrical duct of internal radius R (= 50 mm in the experiment) fitted axisymmetrically with a thin-walled, circular cylindrical hood of internal radius $R_h=1.25R$, length $\ell_h=2R$ and wall thickness $\ell_w=0.06R$, with an *unflanged* opening. The individual hood characteristics are defined in Table 1.

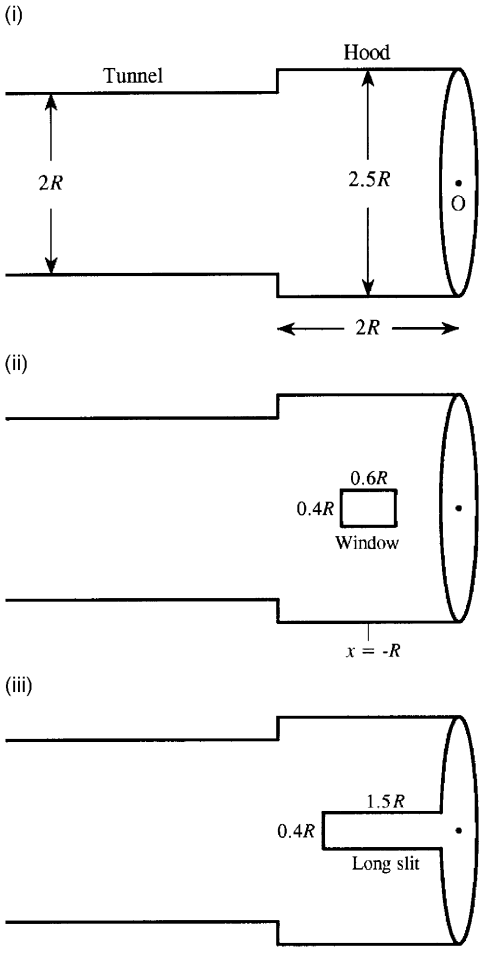

Fig. 2. Schematic of the three experimental short hoods of length $\ell_h=2R$: (i) unvented, (ii) one window with $\ell_x=0.6R$, $\ell_\theta=0.4R$, (iii) long slit with $\ell_x=1.5R$, $\ell_\theta=0.4R$.

Table 1
Hood window characteristics

Hood	Windows	Comments
(i)	None	
(ii)	One: $\ell_x = 0.6R,\ \ell_\theta = 0.4R$	
(iii)	Slit: $\ell_x = 1.5R,\ \ell_\theta = 0.4R$	Modelled numerically as two equal adjacent windows with $\ell_x = 0.75R$

2.2. The model scale experimental train

The circular cross-section of the axisymmetric train has constant radius h and area $\mathscr{A}_o = \pi h^2$ except within a distance L of the front of the train, where the area $\mathscr{A}_T(s)$ varies with distance s from the nose tip. The nose region is ellipsoidal with radius

$$r = h\sqrt{\frac{s}{L}\left(2 - \frac{s}{L}\right)}, \quad 0 < s < L, \tag{1}$$

so that, near the front of the train

$$\frac{\mathscr{A}_T(s)}{\mathscr{A}_o} = \begin{cases} \dfrac{s}{L}\left(2 - \dfrac{s}{L}\right), & 0 < s < L, \\ 1, & s > L. \end{cases} \tag{2}$$

The overall length of the experimental train was 1242 mm, and

$$h = 22.35\,\text{mm}, \quad L = 67.05\,\text{mm}, \tag{3}$$

making the nose 'aspect ratio' $= L/h = 3$. In this case the 'blockage' $\mathscr{A}_o/\mathscr{A} = 0.2$, where $\mathscr{A} = \pi R^2$ is the cross-sectional area of the tunnel, which corresponds approximately to the situation at full scale. The experimental train was fitted with a similarly shaped 'tail' which, however, does not contribute to the formation of the compression wave-front. Eq. (2) may therefore be assumed to apply for all $s > 0$ when used for calculating the compression wave-front.

3. Laboratory measurements

3.1. Experimental apparatus

Model scale experiments were conducted at the Railway Technical Research Institute in Tokyo using the apparatus illustrated schematically in Fig. 3. It is similar to that used by Howe et al. [2] to investigate compression wave formation, but with improvements that permit operation at much higher train speeds in a longer tunnel. In the present experiment the uniform section of the tunnel consists of a 7 m long horizontal, circular cylindrical pipe made of hard vinyl chloride, with inner and outer diameters, respectively, equal to 100 and 114 mm. The axisymmetric model train is projected into the tunnel by means of a four-stage friction drive 'launcher' involving four pairs of vertically aligned wheels; the train was guided along a 5 mm diameter taut steel wire extending along the tunnel. The maximum possible launch speed is about 500 km/h (Mach number $\sim$0.41), the actual speed being controlled by varying the rates of rotation of the drive wheels.

The hood consists of a circular cylindrical, vinyl chloride pipe of inner and outer diameters equal to 125 and 131 mm, and of wall thickness 3 mm (so that $\ell_w = 0.06R$). A 106 mm long collar at the inner end of the hood facilitates an airtight and smooth mating with the circular cylindrical tunnel. When in place the hood and collar have an overall length of 206 mm, and the 'working length' ℓ_h of the hood is 100 mm. The overall length of the tunnel and hood ($\sim$7.2 m) was chosen to ensure that measurements of the compression wave were not influenced by reflections from the distant tunnel exit. The three hood types (i)–(iii) of Fig. 2 were realized by cutting a horizontal slot of azimuthal width 20 mm in the hood wall, extending inwards from the entrance

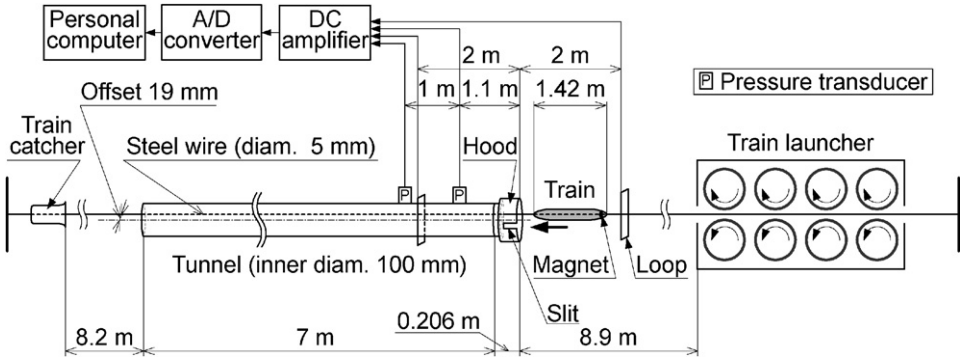

Fig. 3. Schematic of the experimental apparatus.

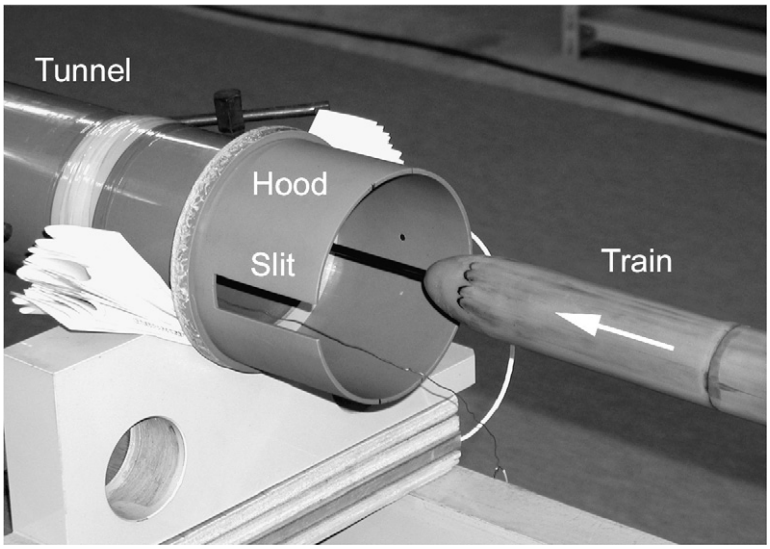

Fig. 4. Hood (iii) with an axisymmetric model train travelling along the 'far' track.

plane an axial distance of 75 mm; the 'open' section of the slot was adjusted by inserting prefabricated, flush-fitting inserts at both ends of the slot. Care was taken to ensure smooth and airtight fits of the inserts.

There is an 8.9 m long 'open' section between the launcher and the hood, which is large enough to ensure that spherically spreading pressure waves generated during the rapid acceleration of the train are negligible at the hood entrance. On emerging from the far end of the tunnel the train is brought to rest without damage by a 'catcher' that slides along the steel wire.

The model train was an axisymmetric body fabricated from a nylon plastic material to the size and shape specified in Section 2.2. The steel guide-wire passes axisymmetrically through a cylindrical hole of diameter 5.5 mm in the model. The wire was displaced a distance of 19 mm from the tunnel axis either towards or away from the slot in order to simulate respectively 'near' and 'far' operations in a double-track tunnel. The photograph (Fig. 4) shows the arrangement for hood (iii) when the train is far from the slit. For these dimensions the blockage $\mathscr{A}_o/\mathscr{A} = 0.2$ (or 0.198 if account is taken of the cross-sectional area of the guide-wire), which is typical of the larger values arising in practice, where for high-speed operations ($U > 200\,\mathrm{km/h}$) $\mathscr{A}_o/\mathscr{A}$ is usually restricted to the range 0.12–0.22.

The standard tunnel cross-section on the Japanese high-speed Shinkansen is $63\,\mathrm{m}^2$. When this is doubled to take account of the image tunnel in the ground plane, the equivalent circular cylindrical tunnel has radius 6.35 m. It therefore follows that, when the model scale radius $R = 50\,\mathrm{mm}$, the tests reported here are at $\frac{1}{127}$ of full scale.

3.2. Measurement procedures

Small permanent magnets made of neodymium were inserted in the tail of the model train. The train speed was measured by detection of the magnetic field as the tail passed through two wire loops (see Fig. 3) placed 4 m apart, one in front and the other to the rear of the hood entrance.

The pressure within the tunnel was measured by two *Kulite Semiconductor Products XCS-190-5G* transducers, flush mounted in the tunnel wall at distances of 1.1 and 2.1 m from the entrance plane of the hood. The pressure data were passed through a *TEAC SA-59* amplifier, digitized using a 12-bit analogue-to-digital converter with a sampling rate of 25 kHz per channel, and stored in a personal computer. The pressure gradient ($\partial p/\partial t$) was calculated using a simple central difference scheme after high-frequency components (>4 kHz) of the measured pressure were removed using a fast Fourier transform algorithm.

The measurements were made over a period of about a month during which weather conditions varied considerably. The temperature and atmospheric pressure were recorded for each experimental 'run' and later used to calculate the mean air density from the equation of state of an ideal gas. This was needed for use in the theoretical equations. The overall error of the speed measurement is estimated to be no more than about 0.5%. It was also estimated that the tolerance error in the train cross-section is about 1%. Hence, because the compression wave amplitude is proportional to $U^2\mathscr{A}_o/\mathscr{A}$, it can be concluded that the overall errors in measurements of the pressure and pressure gradient are, respectively, of order 2% and 3%.

4. The unvented hood

4.1. Formal representation of the pressure wave

The rapid algorithm of [1] predicts the initial form of the compression wave in the tunnel just ahead of the entering train. In this region the unsteady pressure p rapidly reduces to a plane propagating wave and can be expressed in the form

$$p = \frac{\rho_o U^2}{(1-M^2)}\frac{\mathscr{A}_o}{\mathscr{A}}\left(1+\frac{\mathscr{A}_o}{\mathscr{A}}\right)\mathscr{F}\left(t+\frac{x}{c_o}\right). \tag{4}$$

In this formula ρ_o, c_o are, respectively, the mean density and sound speed of the air in the tunnel, $M = U/c_o$ is the train Mach number, and $\mathscr{F}(t+x/c_o)$ is a nondimensional function (exhibiting a weak dependence on Reynolds number) that describes the compression wave profile and accounts for the details of the interaction of the train nose with the tunnel-hood portal and with turbulence in the separated flow over the train to the rear of the nose (see Ref. [1] for further details).

The wave profile is only weakly dependent on the value of the sound speed c_o, which we shall take to be 340 m/s. However, the dependence on mean density ρ_o is more critical; the recorded mean air density varied in the range 1.154–1.194 kg/m^3 during the period of about a month when the measurements were made, and proper account must be taken of this in Eq. (4) when comparing theoretical predictions with experiment.

To understand the theoretical dependence on turbulence friction it is convenient to refer forward to the results shown in Fig. 5 for an unvented hood and to Eqs. (8) and (9). The train nose cuts the entrance plane $x = 0$ of the hood at $t = 0$. The experimental and theoretical pressures are plotted as functions of the nondimensional time $U[t]/R$, where $[t] = t + x/c_o$ is the nominal retarded time. In both cases shown in the figure the main pressure rise is complete at $U[t]/R \approx 4$, following which the pressure continues to rise slowly and effectively as a *linear* function of the retarded time. The characteristics of the main pressure rise at the wave-front are independent of the viscosity and thermal conductivity of the air, so that there is dynamic similarity with full scale at equal values of the Mach number. However, the subsequent linear pressure increase is proportional to the frictional drag distributed over the cylindrical sections of the train and walls of the hood and tunnel wetted by the turbulent flow; the lengths of these sections increase linearly with time and are

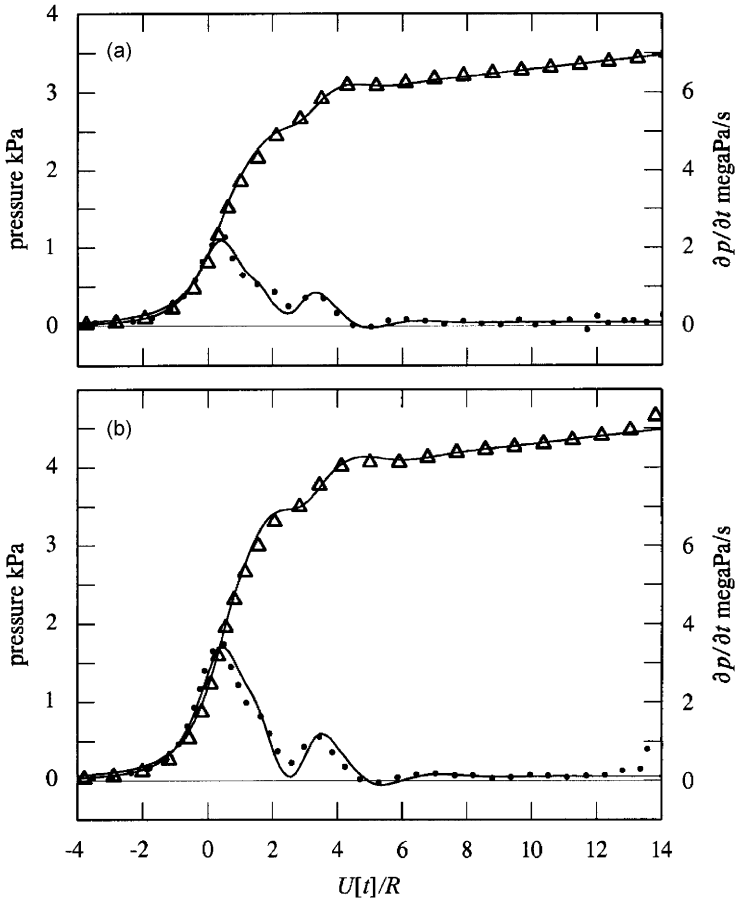

Fig. 5. Measured pressure (△△△) and pressure gradient (• • •) profiles and corresponding predictions (——) for hood (i) and the model scale ellipsoidal train nose defined by Eqs. (1)–(3) when $z_t = 0.38R$: (a) $U = 349\,\mathrm{km/h}$, $\rho_o = 1.194\,\mathrm{kg/m^3}$; (b) $U = 400\,\mathrm{km/h}$, $\rho_o = 1.182\,\mathrm{kg/m^3}$.

approximately equal to $Ut - L$ at time t after the passage of the train nose into the hood (Fig. 1b). The surface drag per unit wall area is nominally equal to $\rho_o v_*^2$ where v_* is the wall friction velocity (which takes different but approximately constant values for the surfaces of the train and the tunnel). In calculating the drag (using equations equivalent to Eqs. (8) and (9)) it is assumed that $v_* = \mu U_\infty$ where U_∞ is the mean flow velocity relative to the respective surface and μ is a friction factor which is taken to be constant. Because the Reynolds numbers at model and full scale cannot normally be the same there cannot be perfect similarity in the turbulence drag component of the pressure rise. The best overall agreement between model scale measurements and the predicted drag component of the pressure is obtained by taking $\mu = 0.053,\ 0.047$, respectively, for the two cases where $U \sim 350,\ 400\,\mathrm{km/h}$ (see Ref. [1]), and these values are used in the results reported in this paper.

4.2. Comparison of theory and experiment for Hood (i)

Fig. 5 illustrates a comparison of theory and experiment for hood (i) and the ellipsoidal nose train defined by Eqs. (1)–(3) with track offset $z_t = 0.38R$ for the two cases:

(a) $U = 349\,\mathrm{km/h}$ $(M = 0.29)$, $\quad \rho_o = 1.194\,\mathrm{kg/m^3}$,

(b) $U = 400\,\mathrm{km/h}$ $(M = 0.33)$, $\quad \rho_o = 1.182\,\mathrm{kg/m^3}$.

The pressure p and the pressure 'gradient' $\partial p/\partial t$ are plotted against $U[t]/R$, where $[t]=0$ as the nose enters the hood. The variations in the pressure gradient govern the subjective influence of the wave in the tunnel, and would also determine the amplitude of the micro-pressure wave in the absence of nonlinear wave steepening. Theory and experiment are in accord up to $U[t]/R\sim 14$, after which the measurements are affected by the passage of the train nose past the pressure transducer.

4.3. Formulae for the compact approximation

The pressure wave begins to form just before the train nose enters the hood. The nose crosses the hood in time $\sim 2R/U$ and the wave-front is fully formed when $t\sim 4R/U$, which is fast enough for the initial displacement of air in the portal to be regarded as irrotational. The characteristic width of the wave-front is roughly the same as the width of the first peak in $\partial p/\partial t$, i.e. of order $2R/M$, which is about three times the length of the hood. This suggests that it might be permissible to regard the hood as being acoustically compact for the purpose of calculating the compression wave. To check this hypothesis we must first recall the appropriate compact-hood formulae for the compression wave.

In the compact approximation the irrotational, wave-front component of the pressure, p_I say, is determined by Howe et al. [2] and Howe [3]

$$p_I(x,t)\approx\frac{\rho_o U^2}{\mathscr{A}(1-M^2)}\left(1+\frac{\mathscr{A}_o}{\mathscr{A}}\right)\int_{-\infty}^{\infty}\frac{\partial\varphi^*}{\partial x'}(x',0,z_t)\frac{\partial\mathscr{A}_{\mathrm{T}}}{\partial x'}(x'+U[t]-M\ell')\,\mathrm{d}x', \tag{5}$$

where $\varphi^*(\mathbf{x})$ is the unique solution of Laplace's equation that represents the velocity potential of a hypothetical, uniform incompressible flow *out* of the tunnel and hood satisfying

$$\left.\begin{aligned}\varphi^*(\mathbf{x})&\approx x-\ell' \qquad \text{for } |x|\gg R \text{ inside the tunnel,}\\ &\approx -\mathscr{A}/4\pi|\mathbf{x}| \quad \text{for } |\mathbf{x}|\gg R \text{ outside the portal.}\end{aligned}\right\} \tag{6}$$

The length ℓ' is the Rayleigh *end-correction* of the portal [4,5].

The functional form of $\varphi^*(\mathbf{x})$ is known only for flow from a thin-walled, circular cylindrical portal [3]. In the present case it must be determined numerically (Fig. 6, also only in the benign approximation $\ell_w=0$), from which the end-correction is found to be negative and given by $\ell'\approx -0.17R$. According to Eq. (5) the regions of the most rapid variations of $\partial\varphi^*/\partial x$ govern the shape of the compression wave-front profile, and Fig. 6b illustrates how these variations occur in the vicinities of the hood entrance and the junction of the tunnel and hood.

When the train nose has passed into the tunnel $\partial\varphi^*/\partial x'=1$ for those values of x' in Eq. (5) where $\partial\mathscr{A}_{\mathrm{T}}/\partial x'\neq 0$, so that the irrotational pressure p_I yields an overall *constant* value for the net pressure rise across the wave-front equal to

$$\frac{\rho_o U^2}{(1-M^2)}\frac{\mathscr{A}_o}{\mathscr{A}}\left(1+\frac{\mathscr{A}_o}{\mathscr{A}}\right),$$

which is equal to the coefficient in the 'rapid' representation (4) of the compression wave. The linear rise in pressure to the rear of the wave-front produced by the frictional drag is denoted by $p_D(x,t)$. The total drag increases linearly with time because the length of the turbulent zone ($\approx$ the length of the train within the tunnel and hood) increases at the constant speed U of the train. This very low-frequency pressure wave source may always be regarded as compact and can be expressed as the following special case of the corresponding formulae given in Ref. [1]:

$$p_{\mathrm{D}}(x,t)=p_{\mathrm{DH}}(x,t)+p_{\mathrm{DT}}(x,t), \tag{7}$$

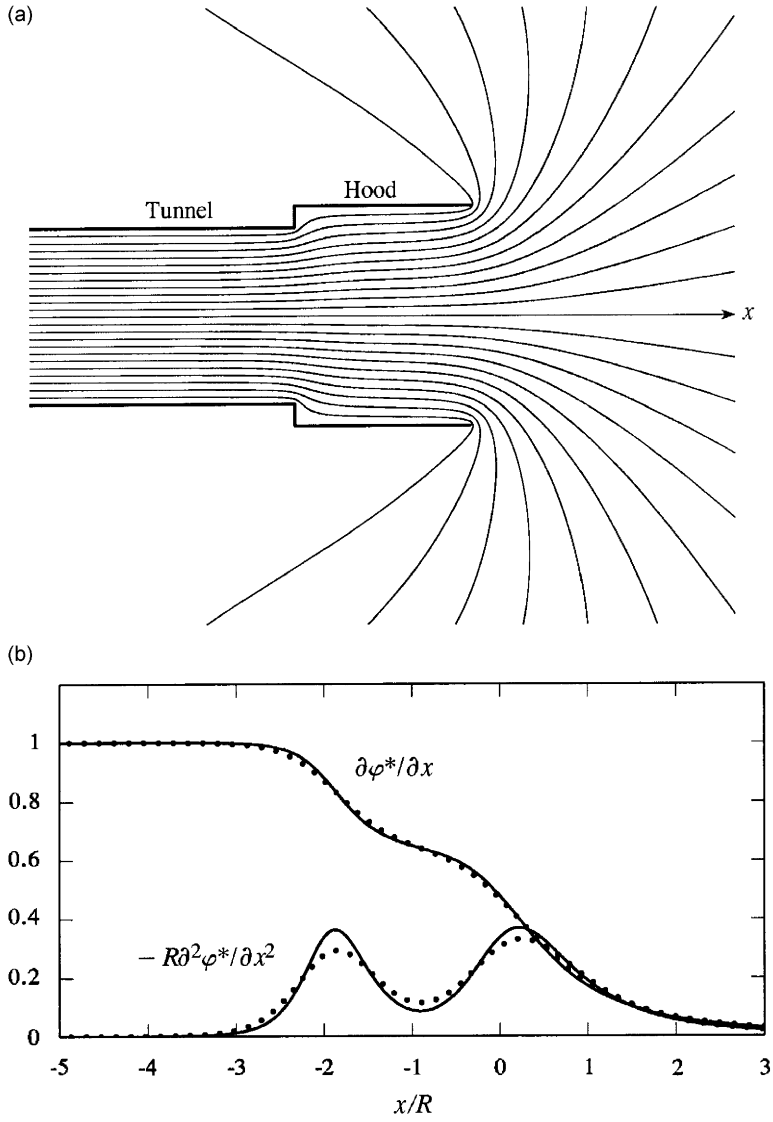

Fig. 6. (a) The streamline pattern for the hypothetical potential flow from hood (i) determined by the harmonic function $\varphi^*(\mathbf{x})$; (b) comparison of the variations of $\partial\varphi^*/\partial x$ and $-R\partial^2\varphi^*/\partial x^2$ along $z_t = 0$ (•••) and $z_t = 0.38R$ (——).

where

$$p_{\mathrm{DH}}(x,t) = \frac{\mu^2\rho_o}{2\mathscr{A}_h}(L_{R_h}U_{\mathrm{HW}}^2 + L_hU_{\mathrm{HT}}^2)\left\{\left[\left(\frac{U(t+x/c_o) - L - M(\ell' - \ell_{\mathrm{E}}\mathscr{A}/\mathscr{A}_h)}{1 - M\mathscr{A}/\mathscr{A}_h}\right)_+ - \left(\frac{U(t+x/c_o) - L - M(\ell' - \ell_{\mathrm{E}}\mathscr{A}/\mathscr{A}_h)}{1 - M\mathscr{A}/\mathscr{A}_h} - \ell_h\right)_+\right] + \left[\left(\frac{U(t+x/c_o) - L - M(\ell' + \ell_{\mathrm{E}}\mathscr{A}/\mathscr{A}_h)}{1 + M\mathscr{A}/\mathscr{A}_h}\right)_+ - \left(\frac{U(t+x/c_o) - L - M(\ell' + \ell_{\mathrm{E}}\mathscr{A}/\mathscr{A}_h)}{1 + M\mathscr{A}/\mathscr{A}_h} - \ell_h\right)_+\right]\right\}, \tag{8}$$

$$p_{\rm DT}(x,t)=\frac{\mu^2\rho_o}{2\mathscr{A}}(L_R U_{\rm TW}^2+L_h U_{\rm TT}^2)\left\{\left(\frac{U(t+x/c_o)-L}{1-M}-\ell_h\right)_+ +\left(\frac{U(t+x/c_o)-L-2M\ell'}{1+M}-\ell_h\right)_+\right\}, \tag{9}$$

in which $(x)_+ = xH(x)$ ($H(x)$ being the Heaviside step function),

$$L_{R_h}=2\pi R_h,\quad L_R=2\pi R,\quad L_h=2\pi h, \tag{10}$$

are the respective perimeters of the hood, tunnel and uniform section of the train, $\ell_{\rm E}=\ell'+\ell_h(1-\mathscr{A}/\mathscr{A}_h)$, and the velocities $U_{\rm TW},\ U_{\rm HW},\ U_{\rm TT},\ U_{\rm HT}$ are defined by

$$U_{\rm TW}=\frac{\mathscr{A}_o U}{(\mathscr{A}-\mathscr{A}_o)}\left\{1-\frac{M\mathscr{A}}{(\mathscr{A}-\mathscr{A}_o)}+\frac{M^2\mathscr{A}(2\mathscr{A}-\mathscr{A}_o)}{2(\mathscr{A}-\mathscr{A}_o)^2}\right\},$$

$$U_{\rm HW}=\frac{\mathscr{A}_o U}{(\mathscr{A}_h-\mathscr{A}_o)}\left\{1-\frac{M\mathscr{A}_h}{(\mathscr{A}_h-\mathscr{A}_o)}+\frac{M^2\mathscr{A}_h(2\mathscr{A}_h-\mathscr{A}_o)}{2(\mathscr{A}_h-\mathscr{A}_o)^2}\right\},$$

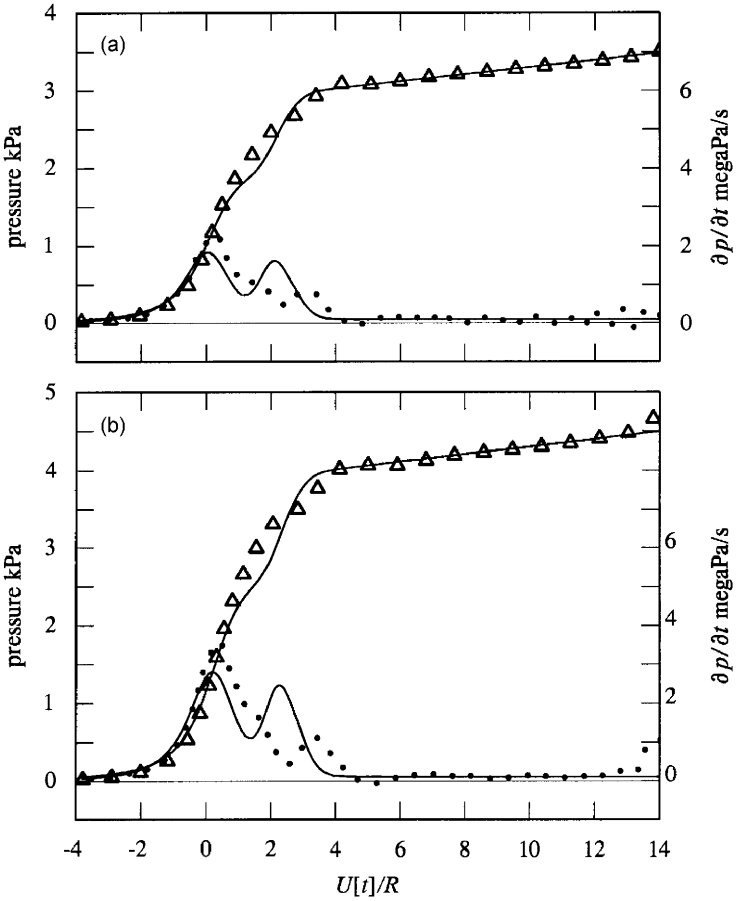

Fig. 7. Measured pressure (△△△) and pressure gradient (•••) profiles compared with predictions of the *compact approximation* (——) for hood (i) and the model scale ellipsoidal train nose defined by Eqs. (1)–(3) when $z_t=0.38R$: (a) $U=349\,\text{km/h}$, $\rho_o=1.194\,\text{kg/m}^3$; (b) $U=400\,\text{km/h}$, $\rho_o=1.182\,\text{kg/m}^3$.

$$U_{\rm TT} = \frac{\mathscr{A}U}{(\mathscr{A}-\mathscr{A}_o)}\left\{1 - \frac{M\mathscr{A}_o}{(\mathscr{A}-\mathscr{A}_o)} + \frac{M^2\mathscr{A}_o(2\mathscr{A}-\mathscr{A}_o)}{2(\mathscr{A}-\mathscr{A}_o)^2}\right\},$$

$$U_{\rm HT} = \frac{\mathscr{A}_h U}{(\mathscr{A}_h-\mathscr{A}_o)}\left\{1 - \frac{M\mathscr{A}_o}{(\mathscr{A}_h-\mathscr{A}_o)} + \frac{M^2\mathscr{A}_o(2\mathscr{A}_h-\mathscr{A}_o)}{2(\mathscr{A}_h-\mathscr{A}_o)^2}\right\}. \tag{11}$$

As already noted (Section 4.1), the absence of Reynolds number similarity between full scale and the model scale experiments implies that model scale predictions of p_D will not necessarily supply the proper contribution of drag to the overall pressure signature at full scale (see Refs. [6,1]).

4.4. Comparison of the compact approximation with experiment

Comparisons of the compact approximation

$$p(x,t) = p_I(x,t) + p_D(x,t)$$

for cases (a) and (b) of Section 4.2 are displayed in Fig. 7. It is evident, that although the compact predictions are qualitatively correct there are significant mismatches in phase and amplitude in the critical region of the compression wave-front, particularly noticeable when theory and experiment are compared for $\partial p/\partial t$. These mismatches are an indication that important contributions to the overall phase of the wave-front are still dependent on multiple reflections, even for such a short hood. These multiple reflections are treated explicitly

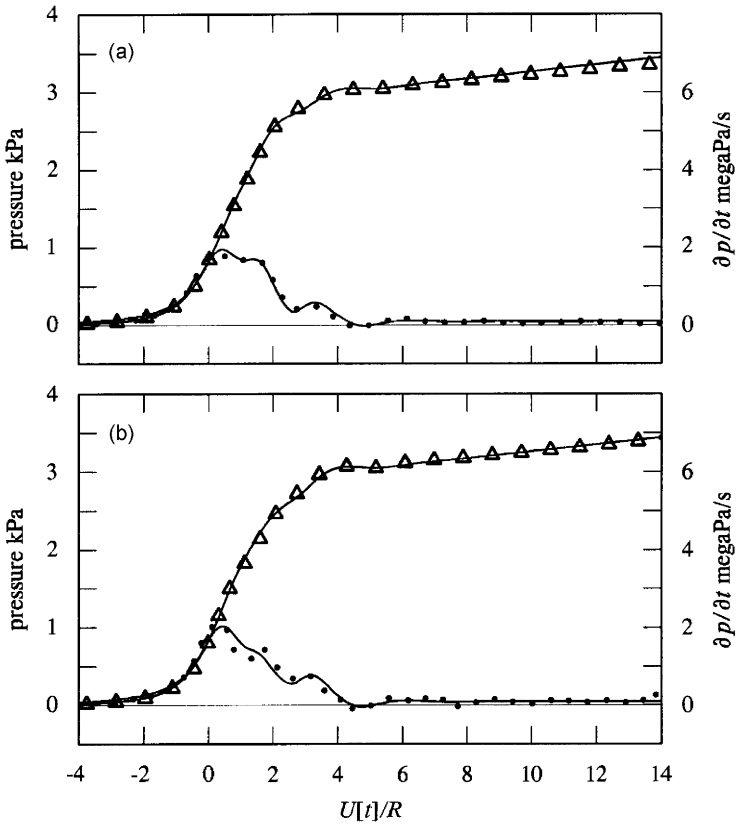

Fig. 8. Measured pressure (△△△) and pressure gradient (• • •) profiles and corresponding predictions (——) for hood (ii) and the model scale ellipsoidal train nose defined by Eqs. (1)–(3) when $z_t = \pm 0.38R$: (a) 'near' window, $U = 350\,\text{km/h}$, $\rho_o = 1.176\,\text{kg/m}^3$; (b) 'far' window, $U = 350\,\text{km/h}$, $\rho_o = 1.174\,\text{kg/m}^3$.

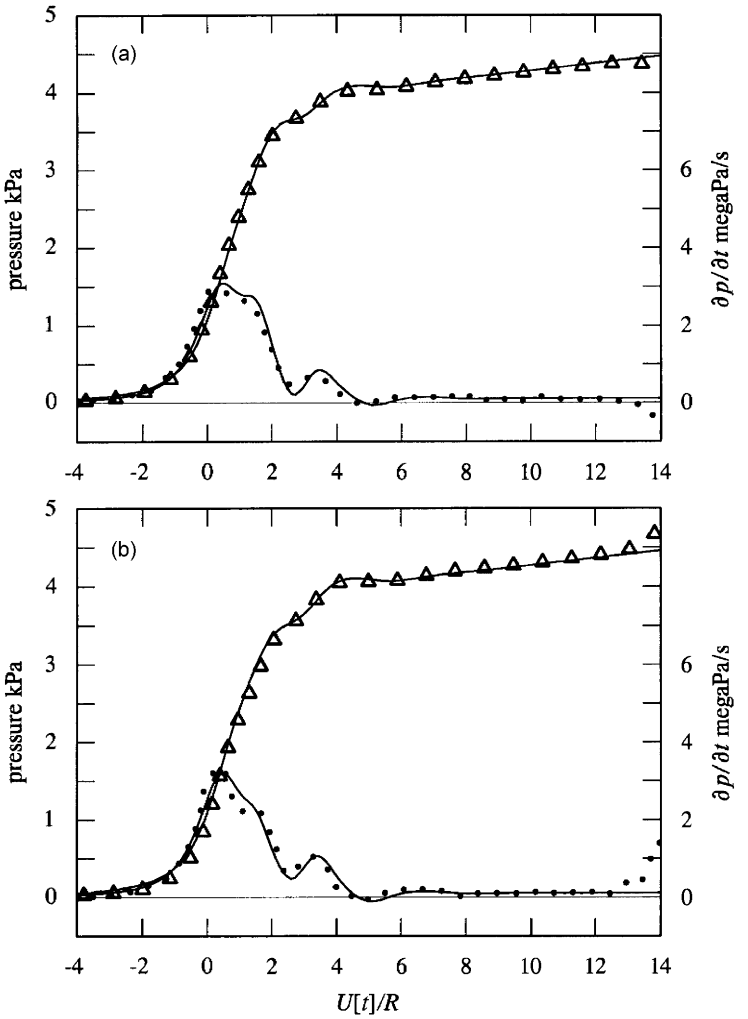

Fig. 9. Measured pressure (△△△) and pressure gradient (• • •) profiles and corresponding predictions (——) for hood (ii) and the model scale ellipsoidal train nose defined by Eqs. (1)–(3) when $z_t = \pm 0.38R$ and $U = 400\,\mathrm{km/h}$: (a) 'near' window with $\rho_o = 1.177\,\mathrm{kg/m^3}$; (b) 'far' window with $\rho_o = 1.173\,\mathrm{kg/m^3}$.

in the rapid algorithm of [1] (as exemplified by the excellent agreement in Fig. 5), but are *not* (of course) included in the compact approximation of Section 4.3. A detailed discussion of the effect on the compression wave of the multiple reflections is given in Section 1.2 of [1].

5. Short hood with a window or slit-opening

5.1. Hood (ii)

Hood (ii) has one rectangular window of sides $0.6R \times 0.4R$ centred on the midpoint of the hood at $x = -R$. Predictions of the rapid algorithm are compared with experiment for near and far windows ($z_t = \pm 0.38R$) in Figs. 8 and 9 when

$$\text{Fig. 8}: \quad U = 350\,\mathrm{km/h}, \quad \text{(a) } \rho_o = 1.176\,\mathrm{kg/m^3}, \quad \text{(b) } \rho_o = 1.174\,\mathrm{kg/m^3},$$

$$\text{Fig. 9}: \quad U = 400\,\mathrm{km/h}, \quad \text{(a) } \rho_o = 1.177\,\mathrm{kg/m^3}, \quad \text{(b) } \rho_o = 1.173\,\mathrm{kg/m^3}.$$

The algorithm determines the acoustic effect of a window in three stages: first a self-consistent calculation is made of the unsteady hydrodynamic volume flow of air through each window; second, this volume flow is used to define the time-dependent strength of an acoustic *point source* located at the position of the nominal centroid of the window in an otherwise rigid-walled hood; finally, the radiation from the source is modelled analytically as two equal amplitude *plane* acoustic waves propagating in both directions in the hood from the source (subsequently experiencing multiple reflections from the ends of the hood and multiple partial transmissions across the hood-tunnel junction into the tunnel).

Such a treatment would be expected to provide a good approximation when the hood length ℓ_h greatly exceeds the hood diameter $2R_h$. The remarkable agreement between theory and experiment exhibited in Figs. 8 and 9 demonstrates, however, that the rapid model continues to be of excellent utility at least down to $\ell_h = 2R < 2R_h$.

5.2. Hood (iii)

Further confirmation of the validity of the rapid algorithm for short hoods is obtained from the comparisons with experiment presented in Figs. 10 and 11 for hood (iii). The 'window' consists of an open-ended slit of length $1.5R$ and width $0.4R$. This is too long to be modelled directly by the 'point source' theory of [1], and the method is applied after first replacing the slit by two equal adjacent rectangular windows of dimensions $0.75R \times 0.4R$, with centroids at $x = -0.375R$ and $-1.125R$.

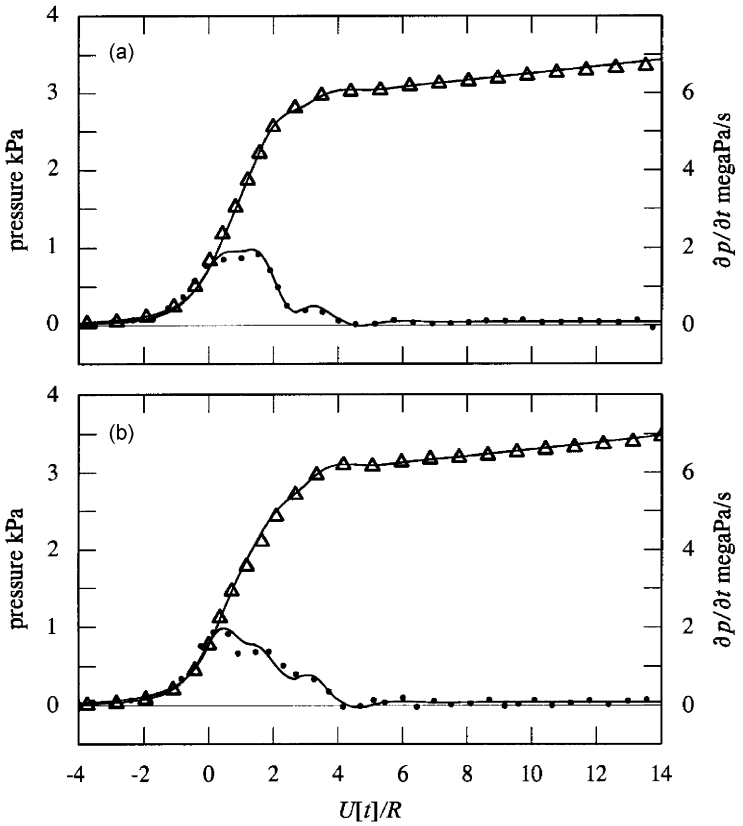

Fig. 10. Measured pressure (△△△) and pressure gradient (• • •) profiles and corresponding predictions (——) for hood (iii) and the model scale ellipsoidal train nose defined by Eqs. (1)–(3) when $z_t = \pm 0.38R$ and $U = 350\,\mathrm{km/h}$: (a) 'near' slit with $\rho_o = 1.171\,\mathrm{kg/m^3}$; (b) 'far' slit with $\rho_o = 1.185\,\mathrm{kg/m^3}$.

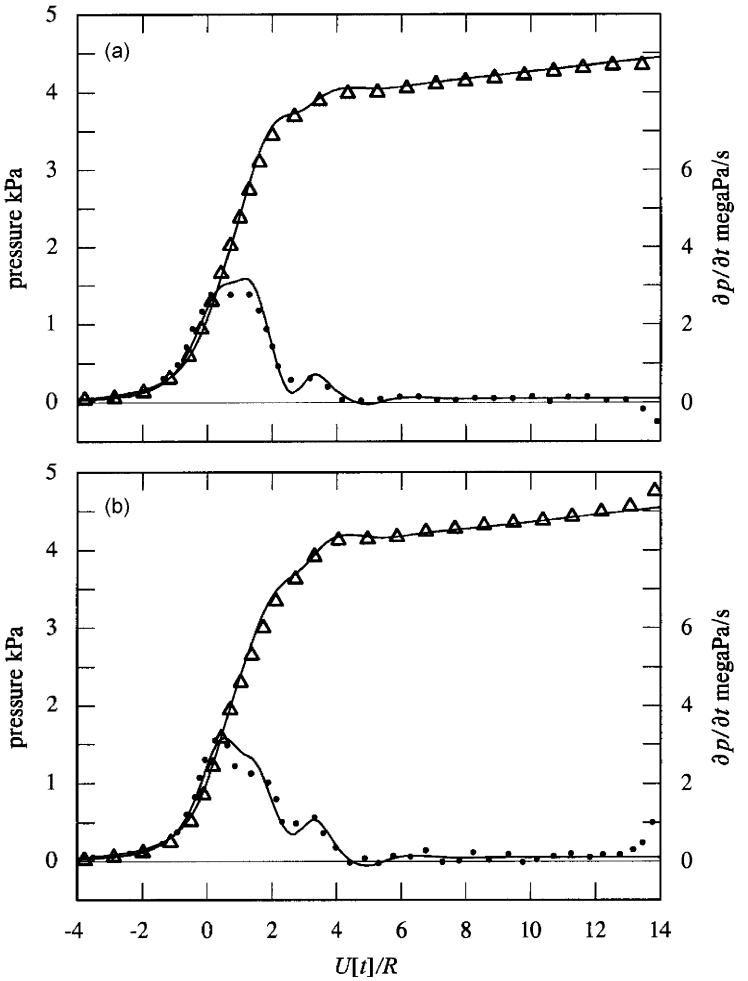

Fig. 11. Measured pressure (△△△) and pressure gradient (• • •) profiles and corresponding predictions (——) for hood (iii) and the model scale ellipsoidal train nose defined by Eqs. (1)–(3) when $z_t = \pm 0.38R$: (a) 'near' slit when $U = 400\,\mathrm{km/h}$, $\rho_o = 1.168\,\mathrm{kg/m^3}$; (b) 'far' slit when $U = 401\,\mathrm{km/h}$, $\rho_o = 1.189\,\mathrm{kg/m^3}$.

The figures, respectively, compare the influences of a near and a far slit on the compression wave for $U = 350\,\mathrm{km/h}$ and $U \sim 400\,\mathrm{km/h}$. In all cases the theory captures the principal features of the wave profiles, in particular the variations of the subjectively important pressure gradient $\partial p/\partial t$.

6. Conclusion

The rapid prediction theory presented in Ref. [1] was originally devised to deal with the problem of compression wave generation by a train entering a long, vented hood, typically of length around 10 times the tunnel height. Acoustically non-compact hoods of this kind will be used more frequently in the future for newer trains operating at very high speeds. For long hoods it is permissible to model the acoustic effect of a window by replacing it by a point source that radiates plane propagating waves within the hood. The same approximation must fail for very short hoods. But, our results confirm that the theory remains applicable for hood lengths as short as $2R$ and train speeds U at least as large as 400 km/h. The thickness of the compression wave-front is then $\sim 6R$ which, although much larger than the hood length, is not large enough for the hood to be regarded as acoustically compact. For such hoods accurate predictions can be made for long slit-like windows (extending over much of the length $2R$ of the hood) by using the 'rapid' algorithm with the slit replaced by a linear array of smaller windows. This is significant because the method may now be applied to

update the designs of the many short hoods already in use on existing networks, for example by means of the optimization procedure proposed by Howe [7].

Acknowledgements

The work reported in this paper is sponsored by the Railway Technical Research Institute, Tokyo, Japan. The authors express their gratitude to Mr. T. Suzuki of Tess Co. Ltd. for his assistance with the model scale experiments.

References

[1] M.S. Howe, M. Iida, T. Maeda, Y. Sakuma, Rapid calculation of the compression wave generated by a train entering a tunnel with a vented hood, *Journal of Sound and Vibration* 297 (2006) 267–292.
[2] M.S. Howe, M. Iida, T. Fukuda, T. Maeda, Theoretical and experimental investigation of the compression wave generated by a train entering a tunnel with a flared portal, *Journal of Fluid Mechanics* 425 (2000) 111–132.
[3] M.S. Howe, The compression wave produced by a high-speed train entering a tunnel, *Proceedings of the Royal Society A* 454 (1998) 1523–1534.
[4] Lord Rayleigh, *The Theory of Sound*, Vol. 2, Macmillan, London, 1926.
[5] M.S. Howe, *Acoustics of Fluid-Structure Interactions*, Cambridge University Press, Cambridge, 1998.
[6] M.S. Howe, M. Iida, Influence of separation on the compression wave generated by a train entering a tunnel, *International Journal of Aeroacoustics* 2 (2003) 13–33.
[7] M.S. Howe, The genetically optimized tunnel-entrance hood, *Journal of Fluids and Structures* (2007), doi:10.1016/j.jfluidstructs.2007.06.005.